Phase accuracy in high-resolution electron microscopy of trigonal and orthorhombic purple membrane

P. A. Bullough and R. Henderson
MRC Laboratory of Molecular Biology, Hills Road, Cambridge CB2 2QH, United Kingdom

ABSTRACT High-resolution images of orthorhombic purple membrane have been obtained by electron cryomicroscopy with spot-scan illumination, and the projection structure at 3.9 Å resolution calculated after image processing and averaging of the data. Since the phases of the structure factors in the projection down the orthorhombic twofold axis should be either 0 or 180°, this offers the first opportunity to make an independent test of the estimated accuracy of high-resolution phases obtained by electron microscopy. The results show the final phases are less accurate than previously estimated by a small factor (1.3). Careful comparison of the new orthorhombic structure to the known trigonal structure shows only small differences after account is taken of a slight difference in the tilt angle of the molecules in the two crystals. This is consistent with the available kinetic and spectroscopic data which show very small differences in behavior.

INTRODUCTION

The purple membrane from *Halobacterium halobium* has been studied extensively (for reviews see Henderson, 1977; Khorana, 1988). An important goal is to determine the three-dimensional structure to atomic resolution. Only then can one hope to understand the mechanism of hydrogen ion translocation, the nature of the interactions between the membrane-bound helices of the constituent protein, bacteriorhodopsin (bR), and the interactions between the protein and the surrounding phospholipids.

Several crystalline forms of bR have been investigated by diffraction techniques (for review see Baldwin et al., 1987) and recent work suggests that high-resolution electron images can be used to determine the structure to high resolution (Henderson et al., 1986; Baldwin et al., 1988; Henderson et al., 1990). Although in principle, electron microscopy of biological molecules should provide structural information to near atomic resolution, in practice images of radiation-sensitive molecules never show the contrast or resolution predicted on the basis of analysis of electron diffraction patterns of the same specimens. The main cause of image degradation seems to be blurring of images due to radiation-induced movement of the specimen (Hayward and Glaeser, 1980; Henderson and Glaeser, 1985; Bullough, 1990). Baldwin et al. (1988) were able to calculate a projection of the native trigonal form of purple membrane (so called h-PM) to 2.8 Å resolution, but this required selection of a small number of images for processing from a very large number actually recorded (of the order of 1,000 images) on the very stable cryomicroscope at the Fritz-Haber-Institut in Berlin. In Cambridge we have a Philips EM420 electron microscope which we have used to collect high-resolution images with a stable side-entry cold stage (Henderson, R., C. Raeburn, and G. Vigers, manuscript in preparation). Samples of orthorhombic purple membrane (o-PM) have proved to be ideal specimens for testing the methodology. Both Bullough and Henderson (1987), and Downing and Glaeser (1986), working with paraffin crystals at 4 Å resolution, have independently shown that radiation-induced specimen movement can be reduced using a "spot-scan" method of imaging which scans a very narrow illumination beam in a raster across the specimen in order to build up an image. This localizes specimen movements to a small area around the illuminating beam and increases contrast by factors of two to three on average. The proportion of good images is also improved. We show here that use of the spot-scan procedure also improves images of orthorhombic purple membrane when compared with conventional imaging.

In this paper, we compare the projection structures of the native (h-PM) and the orthorhombic (o-PM) forms of purple membrane. The three-dimensional structure of h-PM has been determined to 3.5 Å resolution (Unwin and Henderson, 1975; Henderson and Unwin, 1975; Henderson et al., 1990) and a projection structure has been determined to 2.8 Å resolution (Baldwin et al., 1988). The three-dimensional structure of o-PM has been solved to 6.5 Å resolution by Leifer and Henderson (1983). We now report the determination of the projection structure of o-PM to 3.9 Å resolution using improved

Dr. Bullough's current address is Department of Biochemistry and Molecular Biology, Harvard University, 7 Divinity Ave., Cambridge, MA 02138.

spot-scan imaging and computer processing methods. The structure is very similar to that of the native form and this similarity provides independent confirmation of the validity of the methods used. The o-PM form has been chosen as a test specimen for a number of reasons. Because the phases of the structure factors in the projection should be either 0 or 180°, we have the first opportunity, by using the crystal symmetry, to make an independent test of the estimated accuracy of high-resolution phases determined by electron microscopy. Also, it was hoped that careful comparison of the new o-PM structure with the native h-PM structure might reveal any differences in the lipid arrangement or in protein conformation. However, results suggest that any differences in lipid regions are not detectably above the estimated noise levels and there are only very small differences in protein conformation in the two crystal forms. This is consistent with the available kinetic and spectroscopic data which show very small differences in behavior (Michel et al., 1980*a* and *b*).

METHODS

Specimen preparation

Samples of orthorhombic purple membrane came from a single batch prepared by J. S. Jubb (Leifer and Henderson, 1983). Purple membrane is stable indefinitely if stored at 4°C in the dark with 0.2% sodium azide to prevent bacterial growth. A drop of ovalbumin solution (0.1% wt/vol) was applied to a glow-discharge, carbon-coated grid for 60 s and blotted off. A droplet of membrane suspension was applied for a further 60 s and blotted off, and finally a droplet of glucose solution (1% wt/vol) was applied for 60 s. The combination of ovalbumin and glow discharging gave a large number of unrolled but well-ordered membranes.

Imaging

Conventional flood-beam images were recorded on a Philips EM420 microscope operating at 120 kV using a method based on that of Unwin and Henderson (1975). The C400 computer system (Philips Electronic Instruments, Inc., Mahwah, NJ) interfaced to the microscope has allowed additional software for spot-scan imaging to be written (Bullough and Tulloch, 1990; Bullough, 1990). Spot-scan images were recorded by scanning the specimen with a narrow illuminating beam of some 700 Å diameter. Flood-beam and spot-scan images were recorded at both room temperature and at ~155°C using the side-entry cold stage. Room temperature images were recorded at 36,000 magnification with a dose of 1–2 electrons $Å^{-2}$. Low-temerature images were recorded at 60,000 magnification with a dose of 5–10 electrons $Å^{-2}$. During any one imaging session, flood-beam and spot-scan images were taken alternately from crystals on the same grid.

Imaging processing

Image processing followed the procedure of Henderson et al. (1986). Selected low-temperature images were densitometered with a 10-μm aperture and 10-μm step size covering areas of 5,096 × 5,096 pixels, corresponding to 18,000 unit cells. When comparing the top and bottom, and left and right edges of the digitized area, the spot-scan images display a sharp difference in optical density between exposed and unexposed parts of the film. These edges are adjacent in terms of the fast Fourier transform, and the discontinuity leads to sharp and intense spikes in the image transform. The spikes often interfere with low-resolution spots from the crystal lattice and therefore were removed by smoothing and tapering the densities at the image edges. The image was then compressed by performing adjacent pixel averaging over 2 × 2 pixels. Fourier transforms of such compressed images showed 45–60 independent spots when displayed on a raster graphics device.

Transforms were masked by allowing parts of the transform within a diameter of 15 transform units of each observable diffraction peak to go through unchanged. All other parts of the transform were set to zero. This led to averaging over 150 unit cells. A small central reference patch containing 75 unit cells was extracted from the filtered image. With spot-scan images the reference patch was of a rhomboid shape with sides and included angles such that the area enclosed was coincident with part of a scan line and contained no unexposed parts of the film. Using such reference patches, image distortions were corrected as described (Henderson et al., 1986). A second cycle of image distortion correction was performed by calculating a high averaged filtered image from the corrected image created in the first cycle. A reference patch was extracted from this filtered image and used in the cross-correlation with the original raw image. Phases were extracted from the final distortion corrected image using a mask to weight down areas of poor crystallinity and areas of unexposed film as described (Baldwin et al., 1988).

The contrast transfer function of each image was refined automatically against a set of electron diffraction intensities collected by Baldwin and Henderson (1984) as described (Henderson et al., 1986). The origin shift of the low-resolution phases was refined against this data set of three-dimensional phases previously collected by Leifer and Henderson (1983). The value of the crystal tilt angle and the position of the tilt axis were also refined against these data (Henderson et al., 1986). Any structure factors having z^* values >0.005 $Å^{-1}$ were discarded. Finally, phases from individual images were corrected for the effects of beam tilt misalignment (Smith et al., 1983; Henderson et al., 1986) by using the following method. The projection phases should be 0 to 180° and so observed phases within one image were compared to 0 or 180°, whichever gave the least error, and the phase origin and beam tilt were refined jointly by minimization of the difference between the observed phases and the estimated centrosymmetric phases. Phases from all images were merged and final refinements of the contrast transfer functions performed by minimization of the phase residuals between each film and all the others.

Phases from all images in the merged data set were averaged as described (Henderson et al., 1986). Only spots with a signal-to-noise ratio >1:1 (IQ <8) were included in the averaging. IQ is defined by Henderson et al. (1986) such that the signal-to-noise ratio of the reflection amplitude for IQ grades 1–7 is given by 7/grade. Spots of grade 8 are above background by an amount less than the background. The averaged phases were then set to 0 or 180°, whichever gave the smallest residual. Two estimates of phase error were determined. $\Delta\alpha_c$ was determined as the difference between the symmetry imposed phase of 0 or 180° and the observed combined phase, and $\Delta\alpha_m$ was experimentally determined as $\cos^{-1} m$ where

$$m = \frac{\int P(\alpha) \cos(\alpha - \alpha_{comb})\, d\alpha}{\int P(\alpha)\, d\alpha}.$$

$P(\alpha)$ denotes the combined phase probability distribution for phase α as described by Henderson et al. (1986) and α_{comb} is the observed combined phase. A figure of merit for calculation of the structure was determined as fom = cos ($\Delta\alpha_c$) or fom = cos ($\Delta\alpha_m$), whichever was the lesser. This allowed for the possibility that although a structure factor may have an estimated combined phase very close to 0 or 180°, the phase error

distribution might still be large and should therefore be given a small figure of merit. A projection structure was calculated using the symmetry imposed phases and amplitudes from the electron diffraction data set weighted by the figures of merit (Blow and Crick, 1959; Dickerson et al., 1961).

Calculation of difference maps and estimation of noise

A projection of the native (h-PM) form of purple membrane was calculated to 3.9 Å resolution after allowing for the slight tilt of the bR monomers in this form relative to those in the orthorhombic (o-PM) form (Leifer and Henderson, 1983; Tsygannik and Baldwin, 1987) using high-resolution data from tilted images (Henderson et al., 1990). To compare the structures of the bR monomers in the two crystal forms, the density in the native cell was transformed into the orthorhombic cell using programs written by Bricogne (Bricogne, 1974, 1976; Tsygannik and Baldwin, 1987). A real space subtraction of the densities in the transformed native and orthorhombic projections was then performed. Six specific orientations over a small range of tilt angles and tilt axis directions were examined subjectively but the least difference between the h-PM and o-PM structures was seen for the relative orientations of bR in the two crystal forms found previously by Tsygannik and Baldwin (1987).

The noise in each map was estimated by calculating projections using weighted Fourier terms of the form, $F(hkl) = F(hkl) \sin \Delta\alpha_{fom} e^{i\Psi}$, where $F(hkl)$ is the measured structure factor amplitude from electron diffraction, $\Delta\alpha_{fom}$ is the larger of $\Delta\alpha_c$ or $\Delta\alpha_m$ (in the case of o-PM phases), and Ψ is a random phase. The native noise map, calculated in a similar way but with phases rotated 90° from the native structure, was transformed into the orthorhombic cell after taking into account the factor of 1.3 (see below) and the total noise in the difference map calculated.

RESULTS AND DISCUSSION

The results of spot-scan imaging are summarized in Table 1. The quality of images of each type was assessed in two ways. Firstly, it was determined if optical diffraction spots could be observed by eye in all directions to a resolution of ~8 Å. Secondly, it was determined whether the (0 8) reflection (at 9.4 Å resolution) was clearly visible above the background noise. From observation of electron diffraction amplitudes, this spot should be fairly bright (Michel et al., 1980*a*). For both room temperature and low temperature, six times as many spot-scan images as flood-beam images showed good optical diffraction in all directions. Twice as many spot-scan images as flood-beam images showed the (0 8) reflection clearly above background. Fig. 1 shows a low-temperature spot-scan image and its optical diffraction pattern. The pattern has very bright spots visible by optical diffraction to 7.9 Å resolution.

TABLE 1 Comparison of normal flood-beam and spot-scan images of orthorhombic purple membrane

	Type of image			
	Normal RT	Spot-scan RT	Normal LT	Spot-scan LT
No. of images	24	23	49	50
No. showing good diffraction	2	12	5	28
No. with (0 8) visible	7	13	17	32

RT denotes room temperature; LT denotes near liquid nitrogen temperature.

Four good images were selected for processing and the main image data are summarized in Table 2. Table 3 shows the phase error of the averaged data (with phases set to 0 or 180°) in various resolution ranges. Fig. 2 shows the projection structure of orthorhombic purple membrane calculated from the averaged phases (set to 0 or 180°). The calculation was terminated at 3.9 Å resolution and 220 independent figure of merit weighted Fourier terms were included in the map. The map in Fig. 2 can be compared with previous maps calculated for o-PM. It bears little resemblance in its details to that calculated by Rossman and Henderson (1982) using molecular averaging and phase extension. However, it now seems likely that this calculation was in error (Henderson et al., 1986), partly because Rossman and Henderson could not allow for the different tilts of the bR molecules relative to the membrane in the native and orthorhombic forms. The new 3.9-Å projection shows considerably more detail than the 6.5-Å resolution map obtained by Leifer and Henderson (1983).

Given that the phases of the orthorhombic projection should be 0 or 180°, this work provides the first opportunity to obtain an independent estimate of the true accuracy of the phases in both the native and orthorhombic projections. Table 4 shows the mean residuals from imposed phases of 0 or 180° of *individual* phase measurements of given IQ values for o-PM. Also shown are the mean phase residuals, $|\alpha_o - \alpha_{comb}|$, for *individual* native purple membrane reflections of given IQ and experimentally measured phase α_o. These were calculated using the scheme described by Henderson et al. (1986) in which initial estimates of error of individual phases, based on IQ values, were used as weights in calculating the combined phase probability distribution $P(\alpha)$. α_{comb} was determined from this probability distribution. In tabulating IQ versus mean phase residual, we are assuming that spots with given IQ are equally accurate or inaccurate in both crystal forms and that there is a deterministic relationship between IQ and mean phase error. For o-PM we know that all the phases should be 0 or 180°, and therefore we can estimate the true errors of phases with given IQ. It is clear that these errors (column 1 in Table 4) are slightly larger than those previously estimated for h-PM (column

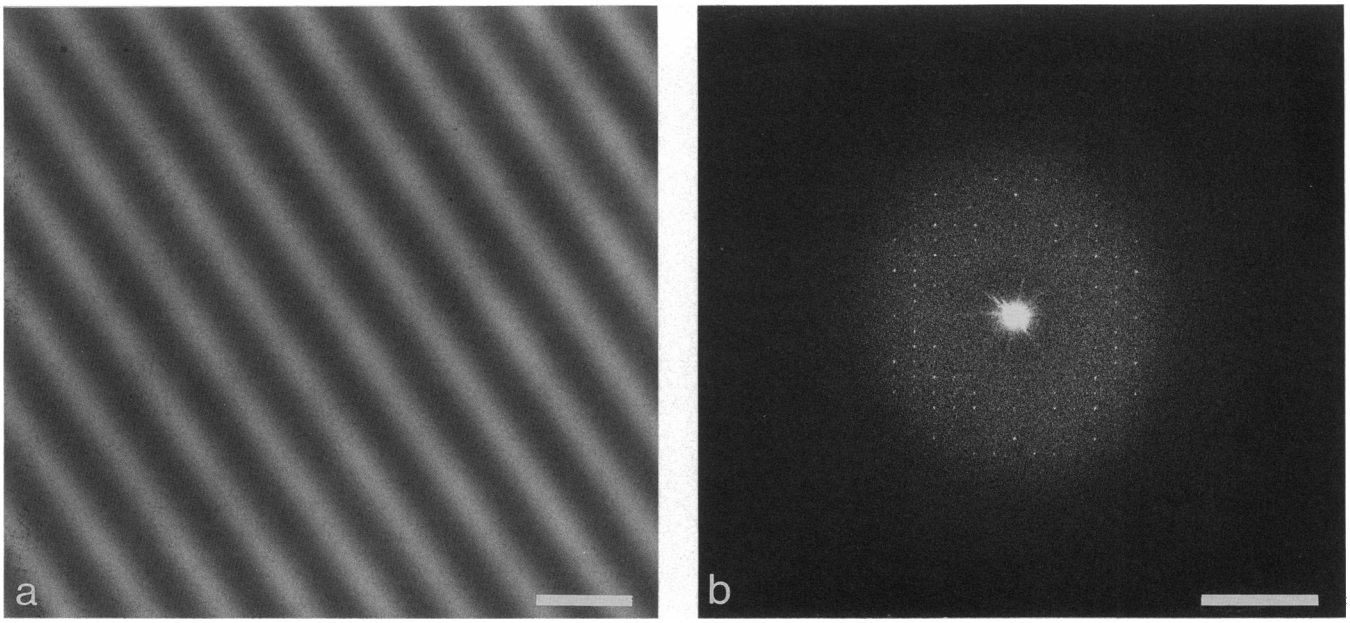

FIGURE 1 (*a*) Typical high-resolution spot-scan image of orthorhombic purple membrane, the lighter areas corresponding to exposed parts of the specimen. Scale bar: 0.1 μm. (*b*) Optical diffraction pattern from an area of the image showing bright spots out to 7.9 Å resolution. Scale bar: 0.1 $Å^{-1}$.

2 in Table 4) by a factor of 1.2–1.3. This factor by which the true errors are increased has been allowed for in the calculation of the noise map of h-PM (Fig. 3 *e*).

Fig. 3 *a* shows approximately one bR molecule (outlined) in the orthorhombic projection, and Fig. 3 *b* shows one bR molecule (tilted by 2°) transformed from the native trigonal cell into the orthorhombic cell. Fig. 3 *c* shows the orthorhombic minus native difference map with the approximate molecular envelope outlined. Corresponding maps of the estimated noise in the three projections are shown in Fig. 3 *d–f*. Given the estimated noise in the o-PM map (Fig. 3 *d*) it is clear that we cannot say anything definitive about the likely positions of lipid molecules in the orthorhombic crystal form because the small peaks that are visible in the lipid region of the map (Fig. 3 *a*) are comparable in height to peaks in the noise map (Fig. 3 *d*). Peaks can be seen in the difference map (Fig. 3 *c*) slightly higher than the estimated noise level (Fig. 3 *f*). However, calculation of the noise level does not allow for uncertainties in the scale and temperature factors between the two structures, and in the true resolution of the orthorhombic structure. Also, the true values of the tilt angles between the two forms of bR relative to the membrane are not known precisely. Although a rough molecular envelope is shown in Fig. 3 *c* it is not certain where the true molecular envelope lies and what the differences in the positions of lipid molecules near the protein surface might be. All of these factors could make the differences observed between the two maps slightly larger than the estimated noise level with-

TABLE 2 Summary of data for each image

Image	No. of phases*	Overall phase residual‡	Weighted residual§	Defocus	Astigmatism	Beamtilt
		degrees	*degrees*	*Å*	*Å*	*mrad*
1505	247	29.39	9.27	1300	1100	1.49
1653	223	39.94	14.78	1250	1050	0.96
1671	196	30.21	11.80	750	1450	0.57
3205	204	39.32	15.14	900	300	2.06

*Resolution is 3.9 Å.
‡Phase residual determined against 0 or 180°.
§Overall weighted residual was calculated using intensity weighted spots as $\Sigma w_i^2 \Delta\alpha_c / \Sigma w_i^2$, where $w_i = 1/(IQ)$.

TABLE 3 Comparison of average phase errors against 0 or 180° and figures of merit in resolution bands

Resolution range	No. of phases	Mean value of $\Delta\alpha_c$	Mean value of $\Delta\alpha_{fom}$	Mean figure of merit
Å		*degrees*	*degrees*	
∞–9.9	34	10.06	12.45	0.93
9.9–7.0	36	9.70	11.19	0.97
7.0–5.7	35	27.01	31.87	0.80
5.7–4.9	37	39.36	47.93	0.63
4.9–4.4	33	38.20	48.82	0.62
4.4–3.9	45	40.96	51.41	0.60
∞–3.9	220	28.17	34.72	0.75

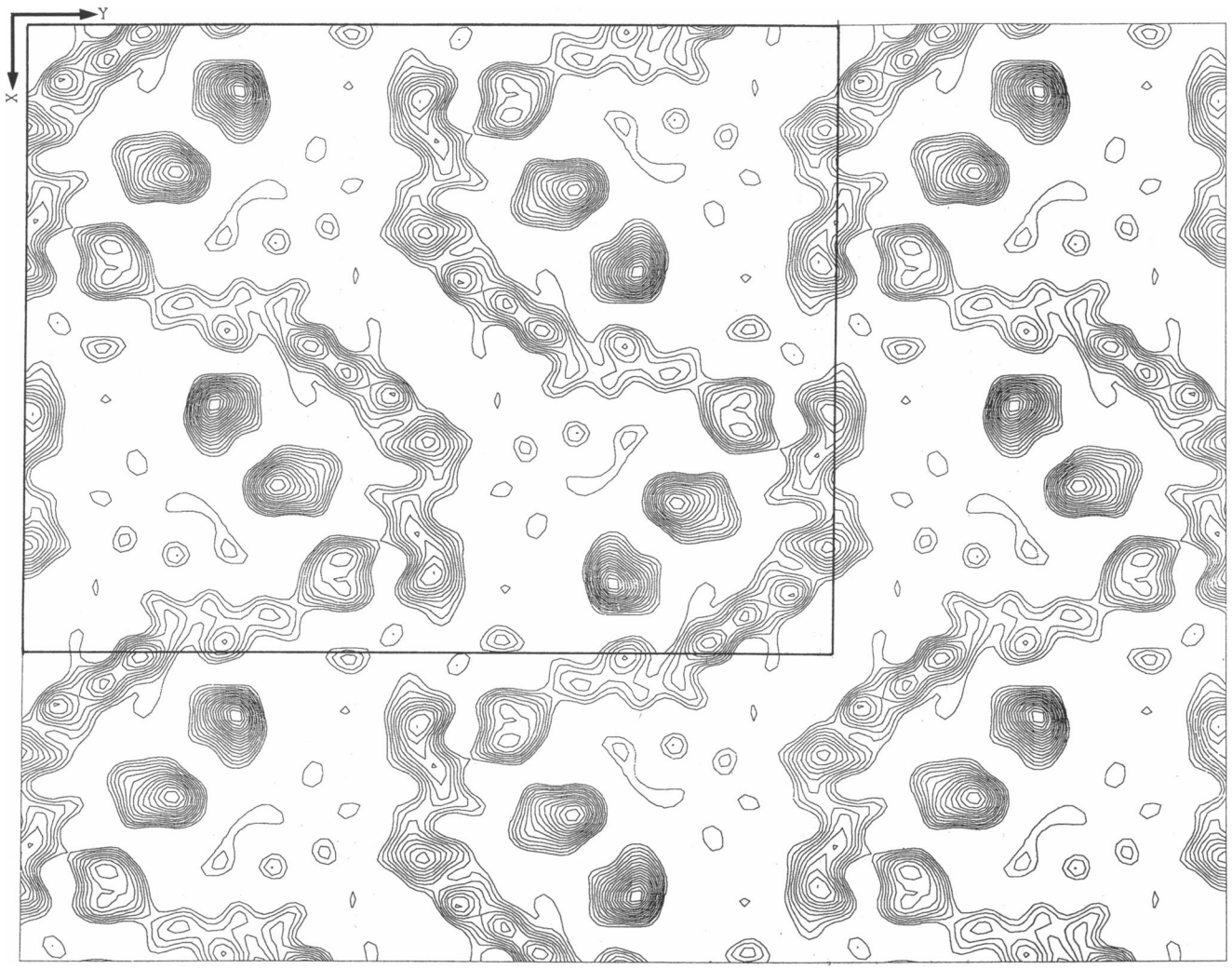

FIGURE 2 3.9-Å resolution projection structure of orthorhombic purple membrane containing 220 Fourier terms in plane group *pgg*. The average figure of merit to 3.9 Å is 0.75. The unit cell has constants $a = 58.7$ Å, $b = 75.5$ Å.

TABLE 4 Mean phase residuals of individual spots

IQ	Mean residual of o-PM phases from 0 or 180°	Mean residual estimated from h-PM distribution*
1	7.74	8.1
2	12.64	10.9
3	27.98	20.1
4	44.53	29.5
5	57.17	40.5
6	64.52	50.9
7	67.51	59.7
8	78.11	82.9

*For the h-PM measurements, the mean residual was calculated as the mean difference from the averaged merged phase for each reflection. These unpublished data were obtained from previous work on h-PM (Baldwin et al., 1988).

out necessarily demonstrating any difference in the protein structures.

A projection of a 2° tilt of the bacteriorhodopsin molecules in the native h-PM cell when compared to the untilted h-PM projection gives peaks in the difference map that are 0.6 times the peaks in the o-PM minus tilted h-PM projection in Fig. 3 *c*. These differences are thus of the same order as the remaining unexplained differences between the h-PM and o-PM projections. However, the tilt is probably real because the features in the h-PM and o-PM projections look subjectively much more similar when the tilt is accounted for.

We conclude that there can only be very small differences in protein structure in the native and orthorhombic forms of purple membrane. If the two structures are compared by eye (Fig. 3, *a* and *b*), the similarity is indeed

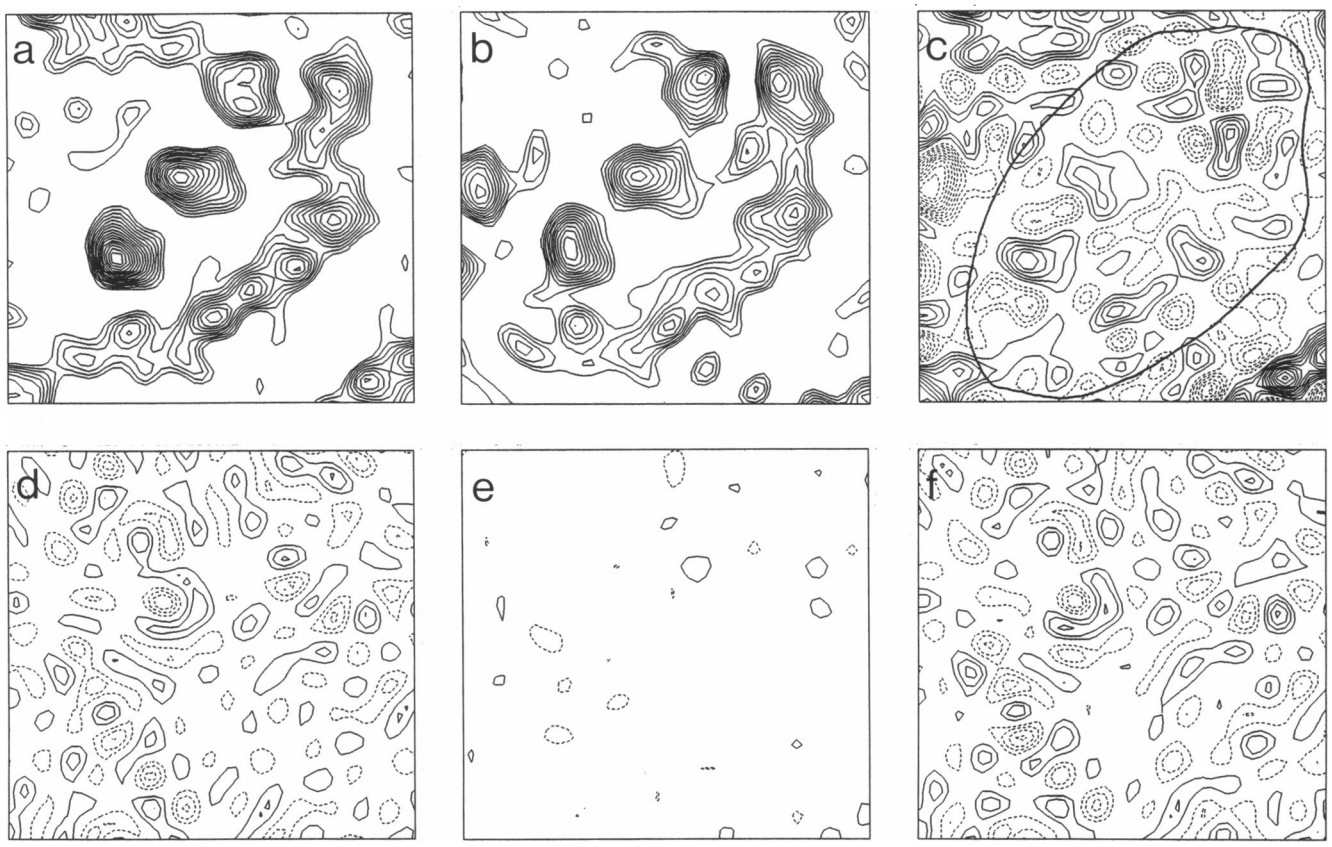

FIGURE 3 Comparison of orthorhombic and native purple membrane projection density maps. (*a*) Orthorhombic projection showing approximately one bR molecule. (*b*) Native form tilted through 2° and with coordinates transformed into the orthorhombic cell. The position, orientation, and scale factor were adjusted to give the closest fit of the densities. (*c*) Orthorhombic minus native difference map. The approximate molecular envelope is outlined. (*d*, *e*, *f*) The estimated noise in each of the projections *a*, *b*, *c*, respectively, with contours at the same level as in the density maps. Note the close similarity of every nuance of the density in *a* and *b*. The noise level in *e* is lower than in *d* because much more work has been done on the p3 crystal form.

remarkable, with most of the peaks and arms of density in the orthorhombic map corresponding to similar features in the native map. This apparent similarity in structure is consistent with the spectroscopic data on the two crystal forms. Michel et al. (1980*a* and *b*) showed that the main difference in spectroscopic properties of the two crystal forms is that the absorption maximum in the visible region is shifted to shorter wavelengths by 5–6 nm in o-PM. This is taken to indicate that the chromophoric region is not significantly different in the two forms. Secondly, the velocity of light-dark adaptation is the same in both native and orthorhombic purple membrane, indicating similar velocities of *cis-trans* isomerization of the bound retinal. The light-dark adaptation is a very sensitive measurement (for example, it changes rapidly with temperature), thus making it unlikely that any significant movements (by the order of 1 Å, for example) are occurring in the protein when it crystallizes in the orthorhombic form.

The apparent similarity between the o-PM and h-PM structures also serves to confirm the method of structure determination by electron microscopy that has been employed in this work and the work on the native form of purple membrane (Henderson et al., 1986; Baldwin et al., 1988). To show any real differences between the two structures, more good data will need to be collected to reduce the noise level in the o-PM map.

CONCLUSION

The use of spot-scan imaging under computer control leads to a substantial improvement in the quality of images of radiation-sensitive specimens. In conjunction with the use of a high-resolution side-entry cold stage to cool the specimen (Henderson, R., C. Raeburn, and G. Vigers, manuscript in preparation), a projection of orthorhombic purple membrane was obtained to 3.9 Å

resolution that showed considerably more detail than previous maps (Michel et al., 1980*a* and *b*; Leifer and Henderson, 1983). However, we are at present unable to say anything about positions of the lipids. Determination of the projection structure of orthorhombic purple membrane to high resolution has provided the first opportunity to make an independent test of the estimated accuracy of high-resolution phases, and results show that final phases are less accurate than previously thought (Henderson et al., 1986) by a small factor of 1.3. Only very small differences in the projection structures of the bR in the native and orthorhombic forms of purple membrane can be discerned. This is consistent with the similar spectroscopic properties of the two forms (Michel et al., 1980*a* and *b*). However, collection of more data to give more accurate phases may yet show more significant differences in the two structures.

The authors are most grateful to J. Baldwin for helpful discussions, C. Raeburn for help with the cold stage, and T. Garrett and P. Rosenthal for a critical reading of the manuscript.

P. Bullough was in receipt of a MRC studentship.

Received for publication 8 February 1990 and in final form 15 May 1990.

REFERENCES

Baldwin, J., and R. Henderson. 1984. Measurement and evaluation of electron diffraction patterns from two dimensional crystals. *Ultramicroscopy.* 14:319–336.

Baldwin, J. M., T. A. Ceska, R. M. Glaeser, and R. Henderson. 1987. Structure analysis of bacteriorhodopsin by electron crystallography. *In* Crystallography in Molecular Biology. D. Moras, J. Drenth, B. Strandberg, D. Suck, and K. Wilson, editors. Plenum Publishing Corp., New York. 101–115.

Baldwin, J. M., R. Henderson, E. Beckman, and F. Zemlin. 1988. Images of purple membrane at 2.8 Å resolution obtained by cryo-electron microscopy. *J. Mol. Biol.* 202:585–591.

Blow, D. M., and F. H. C. Crick. 1959. The treatment of errors in the isomorphous replacement method. *Acta Crystallogr.* 12:794–802.

Bricogne, G. 1974. Geometric sources of redundancy in intensity data and their use for phase determination. *Acta Crystallogr.* A30:395–405.

Bricogne, G. 1976. Methods and programs for direct-space exploitation of geometric redundancies. *Acta Crystallogr.* A32:832–847.

Bullough, P. A. 1990. Imaging of protein molecules: towards atomic resolution. *Electron Microsc. Rev.* In press.

Bullough, P., and R. Henderson. 1987. Use of spot-scan procedure for recording low-dose micrographs of beam-sensitive specimens. *Ultramicroscopy.* 21:233–230.

Bullough, P. A., and P. A. Tulloch. 1990. High resolution spot-scan electron microscopy of an α-helical coiled-coil protein. *J. Mol. Biol.* In press.

Dickerson, R. E., J. C. Kendrew, and B. E. Strandberg. 1961. The crystal structure of myoglobin: phase determination to a resolution of 2 Å by the method of isomorphous replacement. *Acta Crystallogr.* 14:1188–1195.

Downing, K. H., and R. M. Glaeser. 1986. Improvement in high resolution image quality of radiation-sensitive specimens achieved with reduced spot size of the electron beam. *Ultramicroscopy.* 20:269–278.

Hayward, S. B., and R. M. Glaeser. 1980. Use of low temperatures for electron diffraction and imaging of biological macromolecular arrays. *In* Electron Microscopy at Molecular Dimensions. W. Baumeister and W. Vogell, editors. Springer-Verlag, Berlin. 226–233.

Henderson, R. 1977. The purple membrane from *Halobacterium halobium. Annu. Rev. Biophys. Bioeng.* 6:87–109.

Henderson, R., and R. M. Glaeser. 1985. Quantitative analysis of image contrast in electron micrographs of beam-sensitive materials. *Ultramicroscopy.* 16:139–150.

Henderson, R., and P. N. T. Unwin. 1975. Three-dimensional model of purple membrane obtained by electron microscopy. *Nature (Lond.).* 257:28–32.

Henderson, R., J. M. Baldwin, K. H. Downing, J. Lepault, and F. Zemlin. 1986. Structure of purple membrane from *Halobacterium halobium:* recording, measurement and evaluation of electron micrographs at 3.5 Å resolution. *Ultramicroscopy.* 19:147–178.

Henderson, R., J. M. Baldwin, T. A. Ceska, F. Zemlin, E. Beckmann, and K. H. Downing. 1990. A model for the structure of bacteriorhodopsin based on high resolution electron cryo-microscopy. *J. Mol. Biol.* In press.

Khorana, H. G. 1988. Bacteriorhodopsin, a membrane protein that uses light to translocate protons. *J. Biol. Chem.* 263:7439–7442.

Leifer, D., and R. Henderson. 1983. Three-dimensional structure of orthorhombic purple membrane at 6.5 Å resolution. *J. Mol. Biol.* 163:451–466.

Michel, H., D. Oesterhelt, and R. Henderson. 1980*a*. Orthorhombic two-dimensional crystal form of purple membrane. *Proc. Natl. Acad. Sci. USA.* 77:338–342.

Michel, H., D. Oesterhelt, and R. Henderson. 1980*b*. Formation of a new 2-d-crystalline form of purple membrane with orthorhombic lattice. *In* Electron Microscopy at Molecular Dimensions. W. Baumeister and W. Vogell, editors. Springer-Verlag, Berlin. 61–70.

Rossman, M. G., and R. Henderson. 1982. Phasing electron diffraction amplitudes with the molecular replacement method. *Acta Crystallogr.* A38:13–20.

Smith, D. J., W. O. Saxton, M. A. O'Keefe, G. J. Wood, and W. M. Stobbs. 1983. The importance of beam alignment and crystal tilt in high resolution electron microscopy. *Ultramicroscopy.* 11:263–282.

Tsygannik, I. N., and J. M. Baldwin. 1987. Three-dimensional structure of deoxycholate-treated purple membrane at 6 Å resolution and molecular averaging of three crystal forms of bacteriorhodopsin. *Eur. Biophys. J.* 14:263–272.

Unwin, P. N. T., and R. Henderson. 1975. Molecular structure determination by electron microscopy of unstained crystalline specimens. *J. Mol. Biol.* 94:425–440.